46th AIAA Aerospace Sciences Meeting and Exhibit
7 - 10 January 2008, Reno, Nevada

AIAA 2008-502

Receptivity of crossflow instabilities to a periodic roughness array on a swept cylinder: investigation of the roughness size influence

E. Piot*, C. Content†, G. Casalis‡

ONERA DMAE, 2 av. Ed. Belin, BP. 4025, 31 055 Toulouse Cedex, FRANCE

A direct numerical simulation of the flow around a micro-roughness array placed within the laminar boundary layer on a swept cylinder has been performed. Several dimensions of the roughness elements have been investigated. In any case, the quite large value (a few percent of the boundary layer thickness) of the roughness heigth prevents from getting linear receptivity phenomena and requires a computation which takes into account non-linear effects. Both steady and unsteady instability waves are generated downstream of the roughness array, even if the roughness forcing is purely steady. The presence of the unsteady wave may be due to a pocket of absolute instability in the chordwise direction. The unsteady DNS wave fits perfectly with the traveling crossflow wave predicted by the linear stability theory. Its amplitude seems to be fixed by transient effects induced by the numerical initialization procedure. As this amplitude is quite high, this wave interacts non-linearly with the steady wave, which thus does not match exactly with the linear steady crossflow wave. Therefore, the receptivity process cannot be precisely quantified. However, the results enlighten qualitatively the influence of both the roughness heigth and spanwise extent.

Nomenclature

R_c	cylinder radius
Q_∞	incoming velocity
φ	sweep angle
s	chordwise distance
n	wall-normal distance
z	spanwise distance
α	chordwise wavenumber
β	spanwise wavenumber
ω	circular frequency
λ_z	spanwise extent of the computational domain
β_z	spanwise wavenumber associated to λ_z
δ	boundary layer thickness along the attachment line
h	heigth of the roughness element
l_s	chordwise extent of the roughness element

*PhD student, estelle.piot@onera.fr, ONERA DMAE.
†Graduate student, cedric.content@onera.fr, ONERA DMAE.
‡Research Engineer, gregoire.casalis@onera.fr, ONERA DMAE.

l_z spanwise extent of the roughness element

Conventions

DNS Direct Numerical Simulation
LST Linear Stability theory

Superscripts

cyl relative to the smooth cylinder flow (i.e. without roughness element)

I. Introduction

Transition in swept-wing flows is often triggered by a crossflow instability. An overview of this phenomenon can be found in the papers of Arnal,[1]Saric & Reed,[2] Reibert & Saric[3] or Saric, Reed & White,[4] in which the main features of the instability and the way it has been investigated are exposed. Emphasis on the experimental results is provided by the papers of Bippes[5] and Kachanov.[6]

The crossflow instability waves are generated by external disturbances, such as free-stream turbulence or surface roughness. This process is called receptivity. It determines the initial amplitudes of the instability waves, which are then amplified downstream, triggering finally the transition to turbulence. The amplification phase is now well understood, while the receptivity phenomenon is still an open issue. Experiments have shown that crossflow instability admits both stationary and traveling modes. The stationary modes are less amplified than the traveling ones, but local receptivity mechanisms preferably excite stationary modes (see the review of Choudhari & Street[7]). Experiments by Radetzsky *et al.*[8] and by Deyhle & Bippes[9] demonstrate that surface roughness is the primary cause of stationary crossflow vortices. Many papers are thus investigating the receptivity of a swept boundary layer to a surface roughness, or to periodic roughness arrays. But most of the computational and theoretical approaches consider a swept flat plate, neglecting the curvature and/or non-parallel effects. This is the case of the precursor work of Crouch[10] and Choudhari,[11] who both consider the receptivity of Falkner-Scan-Cooke boundary layers as perturbations of a parallel boundary layer. A similar method has been used by Ng & Crouch[12] and shows good agreement with experimental results. But Bertolotti,[13] who uses a Fourier transform approach, shows that including the nonparallel effects strongly modifies the receptivity properties. Collis & Lele,[14] who solve the steady linearized Navier-Stokes equations in the leading-edge region of a swept parabolic body, demonstrate that both nonparallel and curvature effects must be taken into account in the receptivity predictions. This has been confirmed by Janke[15] for both the swept flat plate and swept wing cases.

All these computations require a modelization of the receptivity process. In a previous paper,[16] we performed a three-dimensional direct numerical simulation of the crossflow instabilities generated by a surface roughness periodic array in a subsonic swept boundary layer. This work has shown that a direct numerical simulation is able to capture the receptivity phenomenon, without any specific modelization. The paper also explains which linear stability tools are used to distinguish the resulting instability waves and explains how to evaluate the receptivity coefficient (with help of a method based on the multimode decomposition developed by Tumin[17]).

In this previous work, only one geometry (i.e. height, spanwise and chordwise length) of the roughness elements was investigated. Conversely, the main objective of the present paper is to test different roughness sizes, in order to evaluate the relation between the roughness geometric features and the receptivity coefficient. To the authors knowledge, such a study has never been performed for the crossflow receptivity phenomenon in realistic configuration, the present paper is thus a first attempt.

The outline of this paper is as follows. First, the configuration and the numerical procedure are described. Then, a benchmark case with a given roughness geometry is analyzed and results are compared to those of the linear stability theory. Finally, cases with different roughness geometries are investigated.

II. Configuration and numerical procedure

In this section, the studied configuration and the DNS code are described. They are the same than those presented in our previous paper.[16]

A. Infinite swept cylinder

The leading edge of a realistic swept wing is modelled as an infinite swept cylinder. The cylinder is placed in a uniform and constant incoming flow with the velocity $Q_\infty = 50\,\mathrm{m\,s^{-1}}$. The radius of the cylinder is $R_c = 0.1\,\mathrm{m}$. Two coordinate systems are used for the analysis, as shown in figure 1. The first one (x, y, z) is

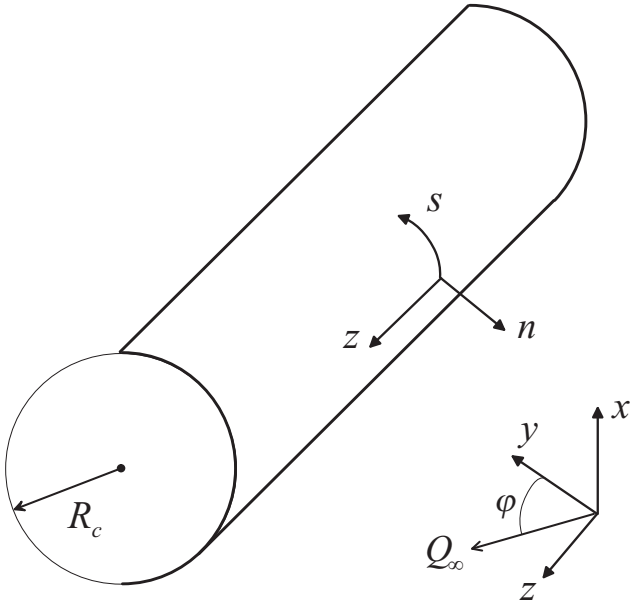

Figure 1. Swept cylinder geometry.

fixed whereas the second one (s, n, z) is a local one linked to the body surface: s represents the arc-length distance on the body from the leading edge and n the distance normal to the wall. For both coordinate systems, z corresponds to the spanwise direction. In the (x, y, z) system, the incoming velocity is given by $(0, Q_\infty \cos(\varphi), Q_\infty \sin(\varphi))$ where the sweep angle φ is equal to 60° in the present study. In the (s, n, z) coordinate system, the three velocity components are denoted as (v_s, v_n, w).

The upstream conditions are given by $p_\infty = 101325\,\mathrm{Pa}$ and $\rho_\infty = 1.18\,\mathrm{kg\,m^{-3}}$ for the pressure and the density respectively. For these numerical values, the leading edge Reynolds number $\bar{R}$ is:

$$\bar{R} = \frac{Q_\infty \sin\varphi \sqrt{R_c}}{\sqrt{2\nu Q_\infty \cos\varphi}} \approx 500 \tag{1}$$

which is (slightly) below the critical value above which the leading edge laminar boundary layer is unstable to the Görtler-Hämmerlin perturbations, see for instance Arnal.[1] Consequently, without large incoming perturbations, the boundary layer may be assumed to be laminar at least in the vicinity of the leading edge.

B. Theoretical laminar flow on the "smooth" cylinder (without roughness element)

In order to determine the "optimal" (in some sense which will be explained hereafter) location of the roughness elements, the stability properties of the theoretical boundary layer which is expected to develop over a cylinder without roughness are investigated. This may be performed in three successive steps. First, with

the assumption of an incompressible flow, an analytical solution exists for the inviscid flow field velocity and corresponding pressure:

$$\begin{aligned} V_s^e &= \left[1 + \frac{{R_c}^2}{(R_c+n)^2}\right] \sin\left(\frac{s}{R_c}\right) Q_\infty \cos\varphi \\ V_n^e &= \left[-1 + \frac{{R_c}^2}{(R_c+n)^2}\right] \cos\left(\frac{s}{R_c}\right) Q_\infty \cos\varphi \\ W^e &= Q_\infty \sin\varphi \\ P^e &= p_\infty - \frac{1}{2}\,\rho_\infty \left(Q_\infty \cos\varphi\right)^2 \frac{{R_c}^2}{(R_c+n)^2}\left[\frac{{R_c}^2}{(R_c+n)^2} - 2\,\cos\left(\frac{2s}{R_c}\right)\right] \end{aligned} \tag{2}$$

Applying these relations at the wall ($n = 0$) provides the wall inviscid flow which can be used as input for a laminar boundary layer computation (second step). Finally this laminar boundary layer is used as input for a linear stability calculation. The latter is performed thanks to the standard Orr-Sommerfeld equation (assuming that the mean boundary layer is weakly dependent on s and neglecting the curvature terms). The eigenmodes (fluctuating velocity components and fluctuating pressure) are searched under the normal mode form:

$$[v_s^f, v_n^f, w^f, p^f] = [v_s(n), v_n(n), w(n), p(n)]\, e^{i(\alpha s + \beta z - \omega t)} \tag{3}$$

where α is a complex number, β the real spanwise wavenumber and ω the real circular frequency. The real part of α corresponds to the chordwise wavenumber, whereas the imaginary part is related to the spatial growth rate of the perturbation: a negative value of the imaginary part means that the perturbation is amplified with respect to s for increasing values of s. Solving the stability problem yields the dispersion relation $\alpha = F(\beta, \omega, s)$. In particular, for a given value of (β, ω), the stability analysis shows that there is a critical (or neutral) distance s_c upstream of which the perturbation is spatially damped, whereas the perturbation is spatially amplified for $s > s_c$.

C. Determination of the roughness array location

An array of roughness elements regularly spaced along the spanwise direction on the surface needs to be placed at some distance from the leading edge. Following experimental results, such as those published by Saric and coworkers,[8] such roughness elements are expected to generate steady crossflow instability modes with a spanwise wavelength identical to the distance between two consecutive roughness elements. Consequently the DNS computation can be performed around a single element in a computational box with a spanwise extent being fixed by the spanwise wavelength, as shown in figure 2. Periodic boundary conditions are enforced at the spanwise boundaries. The location of the roughness elements array has been chosen to be slightly upstream of the critical abscissa s_c.

The linear stability calculations are thus limited to steady modes ($\omega = 0$). Then the "optimal" choice consists in finding the value of β such that:

- the location of the critical abscissa s_c is as small as possible (in order to avoid having a too long stable region)
- the spanwise wavelength $2\pi/\beta$ is as small as possible (in order to reduce the spanwise extent and thus the number of points in the z-direction)
- the corresponding chordwise wavelength $2\pi/\alpha$ is small enough to have a few chordwise oscillations within the computational domain that must not be too large in the s direction.

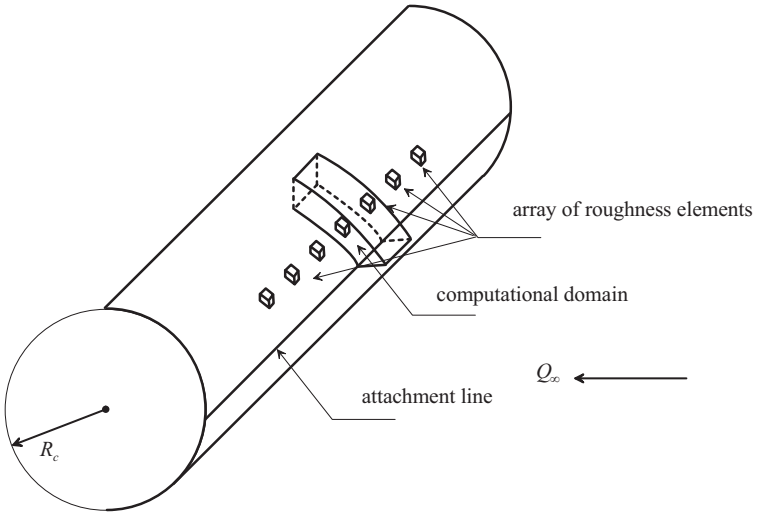

Figure 2. Regularly placed roughness elements at some distance from the attachment line (leading edge). The computational domain contains only one roughness element.

The values of the incoming velocity and of the sweep angle have been actually determined within this optimization process in addition to the constraints to have a stable leading edge with respect to the Görtler-Hämmerlin modes, see Eq.(1), and if possible to be in the range of the values used for the experiments performed by Poll.[18] The chosen values for the incoming velocity and sweep angle are very close to the optimal ones. The final values of the spanwise wavenumber and of the corresponding critical abscissa s_c for steady crossflow waves are given by:

$$\lambda_z = 2\pi/\beta = 13\delta \quad ; \quad s_c = 25\delta$$

where δ is the boundary layer thickness along the leading edge. The dimensions at the wall are displayed in figure 3.

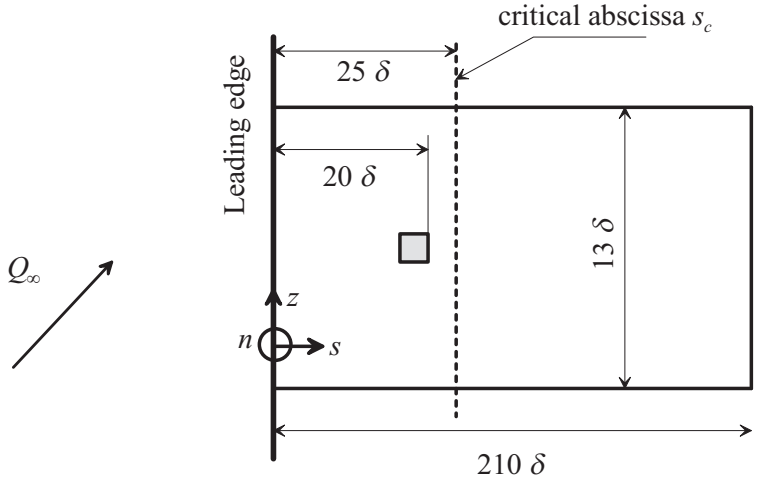

Figure 3. Dimensions of the considered domain at the cylinder surface around a single roughness element. The critical abscissa corresponds to that of the zero frequency instability mode.

As it can be observed, the roughness element is located slightly upstream of the critical abscissa s_c.

D. Numerical procedure

The system of the compressible Navier-Stokes equations is solved numerically using the multi-purpose in-house solver sAbrinA.[19–21] The Navier-Stokes equations are discretized using high-order numerical schemes and structured multi-block meshes. The spatial scheme is a classical fourth-order accurate centered explicit finite difference discretization, while a compact explicit third-order accurate Runge-Kutta algorithm is used for time advancement. The grid is three-dimensional, structured and curvilinear. Eight subdomains are used and one of them corresponds to the roughness element location. For more details on the numerical method and boundary conditions, the reader is referred to our previous paper.[16]

The computation is actually performed in two successive steps. In the first one, the Navier-Stokes equations are solved on the "smooth" cylinder, i.e. without the roughness element. In that case the eighth sub-domain, which corresponds to the location of the roughness element itself, is part of the flow. The inviscid analytical flow field is imposed as initial condition. After some transient a steady flow is obtained, which is called the "base flow". In the second step, the roughness element is present. Therefore the eighth domain is dropped and no-slip boundary conditions are imposed on its surface. The base flow is imposed as initial condition on each mesh point of the remaining seven sub-domains.

The specificity of this computation is thus that the roughness element is meshed and that no-slip boundary conditions are directly imposed at its walls.

E. Roughness element dimensions

As it may be inferred from the previous paragraph, the roughness element is assumed to have a geometry which follows the lines of the mesh. The three dimensions of the parallelepipedic roughness element are denoted by (l_s, h, l_z). Four cases have been analysed in the present study, they are detailed in table 1.

	wall-normal height h	chordwise length l_s	spanwise length l_z
case 1	$\delta/10$	$1.6\,\delta$	$1.625\,\delta$
case 2	$3\delta/40$	$1.6\,\delta$	$1.625\,\delta$
case 3	$\delta/20$	$1.6\,\delta$	$1.625\,\delta$
case 4	$\delta/10$	$1.6\,\delta$	$9.75\,\delta$

Table 1. List of the four considered cases. The three first cases consist in a parametric analysis of the influence of the roughness element height, the fourth case corresponds to a roughness with a large spanwise extent.

Case 1 is the benchmark case widely studied in our previous paper.[16] The chordwise extent of the roughness element has not been changed from one case to another. It corresponds roughly to half of the chordwise wavenumber of the expected steady crossflow mode. This value is expected to correspond to a maximum of receptivity as it has been well established for 2D flows (see former experiments by Saric[22] or DNS computations[23]). This criterion based on the Fourier transform of the spatial shape of the roughness element is applied for the present 3D configuration.

III. Analysis of the first case

In this section, the main results of the benchmark case are given. For a detailed investigation, see Piot *et al.* [16]

A. Laminar flow on the "smooth" swept cylinder

As explained above, the first step consists in computing the flow around the swept cylinder without roughness element by imposing the inviscid flow provided by the analytical relationships given in Eq. (2). As expected,

after some transient, the obtained flow is independent of the spanwise coordinate and is steady. This last observation can be emphasized: even if the obtained mean laminar boundary layer flow is unstable with respect to crossflow instability, the DNS does not exhibit this instability in the case of the perfectly smooth cylinder, i.e. whithout roughness excitation.

B. Unsteady part of the perturbation induced by the roughness element

The second step starts with this flow but now with a roughness element placed on the surface as described above. After a new transient, the different signals coming from positions downstream of the roughness element show that an unexpected unsteady perturbation takes place in the flow. This unsteady part is nearly harmonic with a frequency close to 3400 Hz. It appears thus necessary to decompose the instantaneous flow field into a mean part and an unsteady one simply by performing an average value over a few periods. As the flow is nearly harmonic this average procedure should not induce large numerical bias. The chordwise velocity component is decomposed as:

$$v_s(s,n,z,t) = < v_s >_0 (s,n,z) + v_s^{unst}(s,n,z)\cos(2\pi f t + \phi) \tag{4}$$

where ϕ stands for a phase and $f \approx 3400\,\mathrm{Hz}$. A similar decomposition is used for each velocity component. As described in our previous paper,[16] the unsteady part exhibits a periodicity in the spanwise direction but with twice the expected β_z wavenumber, which is given by the spanwise extent $\lambda_z = 2\pi/\beta_z$ of the computational domain. A linear stability analysis has thus been performed for instability waves corresponding to this $2\beta_z$ spanwise wavenumber. The mean boundary layer flow is very stable with respect to this wavenumber, except for a small range of frequencies that correspond exactly to the one observed in the DNS. In order to confirm that the unsteady perturbation is a crossflow instability mode in the sense of the linear stability theory, the amplitude functions of the velocity components have been calculated for the DNS computation, thanks to a $2\beta_z$ Fourier transform. The resulting Fourier modes are then compared to the normal modes of the linear stability theory (LST) (see Eq. (3) with $\beta = 2\beta_z$ and $\omega = 2\pi f$). The comparison for $s \approx 0.025\,\mathrm{m}$ is plotted

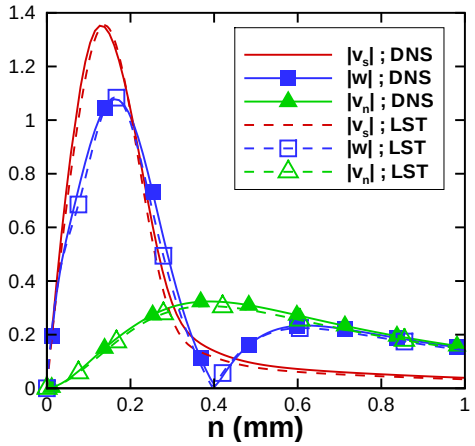

Figure 4. Amplitude functions for the three velocity components associated to the unsteady part of the perturbation. Comparison between the present DNS result and the linear stability analysis. The chordwise location is $s/R_c \approx 14°$.

in figure 4. The vertical axis provides the velocity in $\mathrm{m\,s^{-1}}$ (to be compared to the incoming flow velocity $Q_\infty = 50\,\mathrm{m\,s^{-1}}$). The amplitude of the LST result has been adjusted in order to fit the DNS result. A perfect agreement is obtained which proves the crossflow nature of the unsteady perturbation and which also illustrates the fine resolution of the DNS. It must also be noted that the amplitude of the perturbation is not small so that non linear effects may occur further downstream by "linear" amplification of this perturbation.

C. Steady part of the perturbation

The steady part of the perturbation can now be investigated. Each physical quantity q (velocity component, pressure...) is decomposed according to Eq. (4) and then the mean value is itself decomposed into three parts:

$$< q >_0 (s, n, z) = Q_s^{cyl}(s, n) + q^r(s, n, z) + q^{CF}(s, n, z) \tag{5}$$

where Q^{cyl} corresponds to the quantity for the smooth cylinder flow (first step computation), q^r to the forced perturbation induced by the roughness element and q^{CF} to the eigenresponse, which is the crossflow instability mode in the present study. The $< q >_0$ term is obtained by performing a time-average of the final numerical results (i.e. those obtained by the computation with the roughness element). The q^r and q^{CF} terms cannot be easily distinguished. Let us just mention that the linear stability theory for the given β_z spanwise wave number and for the given (zero) frequency leads to several modes (an infinity). Any perturbation may be represented as a linear combination of all these modes. q^{CF} is only one of them and q^r represents the remaining part of the linear combination. In our previous paper,[16] the multimode-decomposition method (see Tumin[17]) has been applied to $< q >_0$, in order to distinguish q^{CF} and q^r. However, this method does not correctly works in the present case. One possible reason is that non-parallel and surface curvature effects, which are quite significant for the present base flow, are not taken into account by this method. The most likely reason is that the DNS steady flow does not exhibit a linear behavior. As pointed out previously, the amplitude of the traveling crossflow wave is quite high. Therefore, non-linear interactions take place between the unsteady and steady flow field. Figure 5 compares the β_z Fourier transform of $< q >_0 - Q^{cyl}$ to the normal modes obtained by the linear stability theory with $\beta = \beta_z$ and $\omega = 0$). The DNS amplitudes does not look linear. Especially, two bumps can be observed on the DNS chordwise velocity, one of them being located close to the position of maximum velocity for the traveling wave.

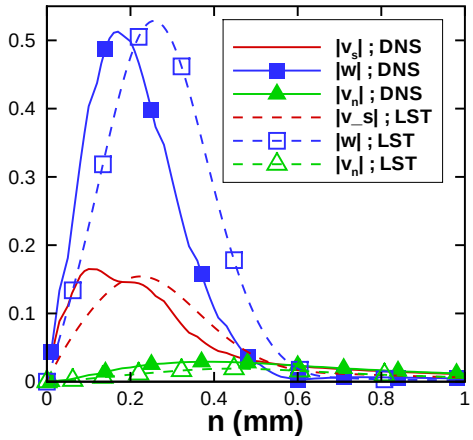

Figure 5. Amplitude functions for the three velocity components associated to the steady part of the perturbation. Comparison between the present DNS result and the linear stability analysis. The chordwise location is $s/R_c \approx 14°$.

Finally, one can assume that the unsteady mode is so large that it induces non-linear behavior which actually drives the steady mode evolution.

IV. Influence of the roughness element size

A. Generation of the steady crossflow wave

The evolution of the perturbation induced by the roughness element $<q>_0 - Q^{cyl}$ is plotted as function of s and z in figure 6. Each case described in Table 1 is displayed. A strong flow deformation can be seen around the roughness location, with different features between the three first cases and the fourth one. Further downstream it appears more or less regular oscillations associated to the β_z spanwise wavenumber. Theses oscillations are similar for cases 1,2 and 4, but are very weak in the third case. In fact, for this case the $2\beta_z$ composant of the flow spanwise Fourier transform is almost as high as the β_z one, which makes the latter hardly visible.

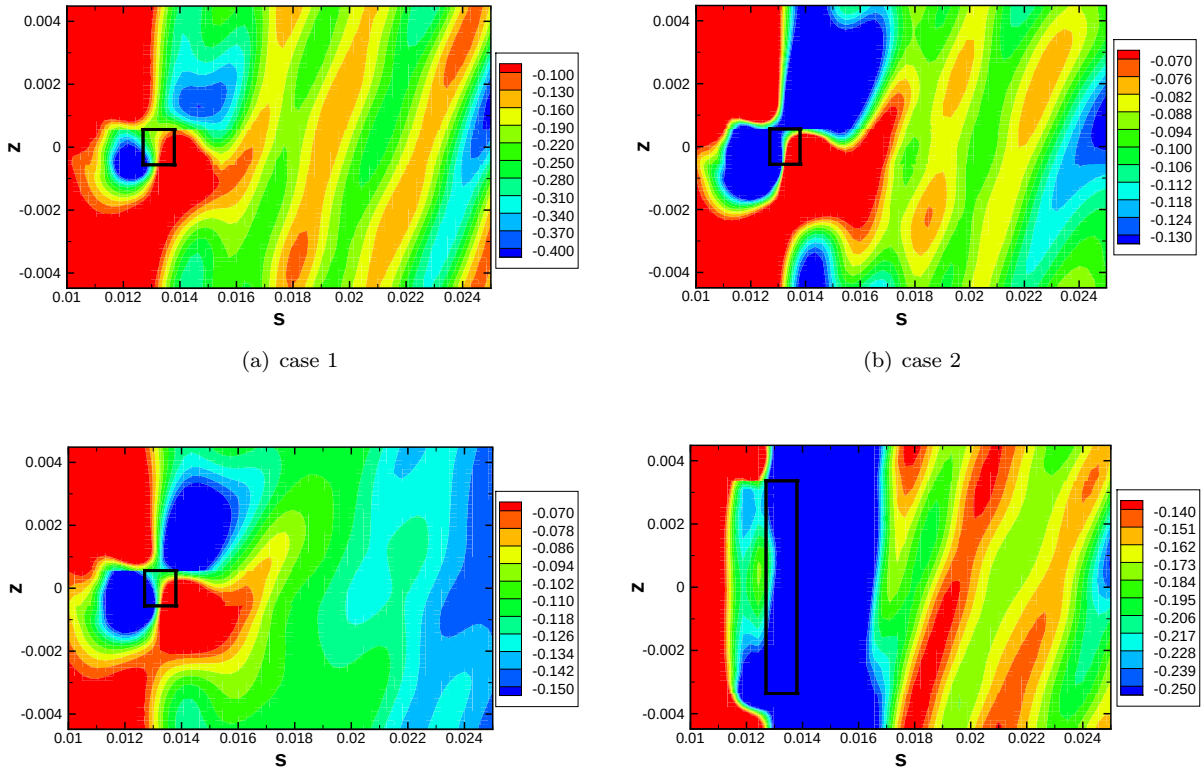

(a) case 1

(b) case 2

(c) case 3

(d) case 4

Figure 6. Steady chordwise velocity $<v_s>_0 - V_s^{cyl}$ at $n = 0.24$mm, i.e. above the roughness top. The roughness element location is plotted as black lines. It must be pointed out that the velocity levels differ from one figure to another.

As explained previously, the steady crossflow modes displayed in figure 6 certainly have a non linear nature. Therefore, trying to extract the pure crossflow mode denoted as q^{CF} in Eq. (5) from the total flow field is pointless. In order to characterize the global effect of the roughness element size on the flow field, it may thus be more realistic to focus on the steady perturbation $<q>_0 - Q^{cyl}$. This leads to the definition of an energy $e(s)$ that reads as:

$$e(s) = \int_z \int_n \sum_{i=1}^{3} (<v_i>_0 - V_i^{cyl} - <<v_i>_0>_z)^2 \mathrm{d}n\mathrm{d}z \tag{6}$$

where v_i stands for every velocity component and $<< v_i >_0>_z$ is the average value in z and time of the DNS flow field. This last term is included in the energy definition to ensure that the integrated function

is zero for the highest n values. This allows thus a meaningful comparison between the four considered cases, which is shown in figure 7. The three first cases correspond to a decreasing height of the roughness

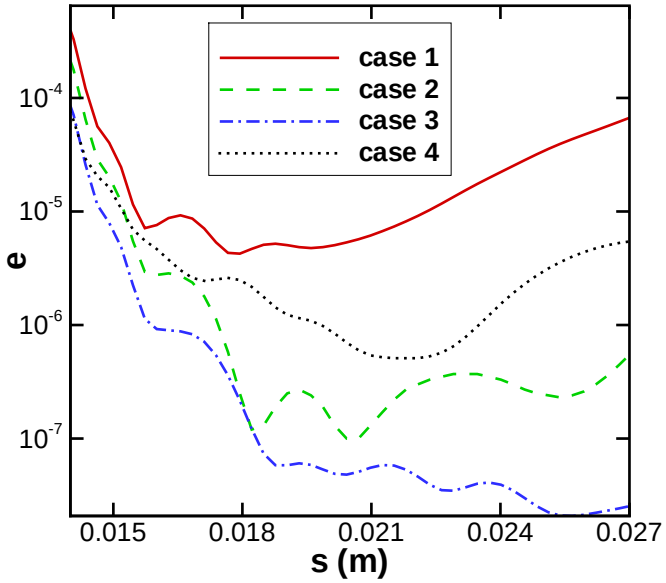

Figure 7. Energy of the perturbation downstream of the roughness element for the four considered cases, see Table 1.

element. The results are in accordance with the expected ones, even if the various s dependencies are not fully intuitive. This is probably due to the non linear effects. Case 4 illustrates the dependency to the spanwise extent of the roughness element and to the spacing between the roughness elements, which is more difficult to interpret, since there is not much knowledge on this issue. However that may be, the roughness size is in every case larger than the critical size below which linear receptivity mechanisms are expected to occur (around one tenth of the boundary layer displacement thickness δ_1 as given by Ng&Crouch,[12] whereas even in case 3, $h \approx 0.3\,\delta_1$). In the studied configurations, the initial amplitude of the steady crossflow mode seems to be driven by the features of the flow distortion in the roughness element vicinity. However, it must be pointed out that for the present computations, the presence of an unwanted traveling crossflow wave influences significantly the steady results, which must therefore be considered with caution.

B. Generation of the traveling crossflow wave

As explained in section III, the unsteady oscillation observed in the case 1 is a traveling crossflow wave with a spanwise wavenumber of $2\beta_z$ and a frequency around $f = 3400\,\mathrm{Hz}$. Its spatial evolution agrees perfectly with the LST results, which moreover shows that this wave is amplified in the chordwise direction. Finally, in agreement with the classical properties of a traveling crossflow wave, the DNS results show that this wave is convected in the chordwise direction. However, the wave persists in time, and consequently is not swept away from the computational domain. To try to understand this characteristic, a linear stability of the base flow (i.e. the smooth cylinder flow) has been performed at various chordwise locations around the roughness position. The chordwise wavenumber has been obtained for several frequencies but for the fixed spanwise wavenumber $2\beta_z$. The imaginary part of α (i.e. the opposite of the chordwise growth rate) is plotted in figure 8. First, one can check that the frequency around 3400 Hz is actually the one that is amplified at first (with respect to the chordwise direction). One can also see that there is a switch in the branch shapes between the lowest and largest s locations. This feature can be a sign of an absolute instability, this is currently

studied. It must be pointed out that this absolute instability is not a pure one, because it is established for artificial $2\pi/\beta_z$ periodic conditions. Consequently, it is an absolute instability in the chordwise direction only.

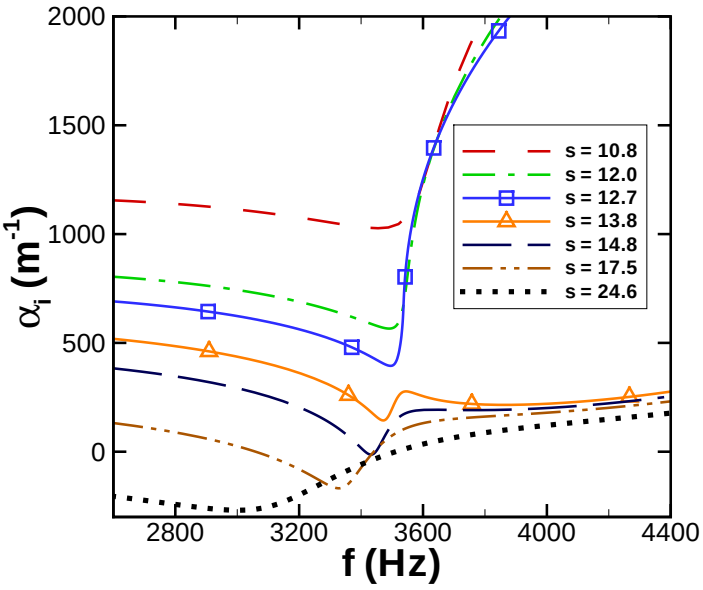

Figure 8. Imaginary part of the chordwise wavenumber vs frequency. Results from the linear stability analysis of the smooth cylinder flow, for a spanwise wavenumber of $2\beta_z$. The chordwise locations s at which this analysis has been performed are given in mm. The lines with square symbols (respectively triangles) correspond to the s values of the upstream (respectively downstream) side of the roughness element.

This could explain the persistence of the traveling wave. Indeed, the final computation is initialized with the smooth cylinder flow. Consequently, imposing a no-slip condition at the roughness surface generates transients in the computation. These transients excite the absolute instability, in a small pocket around the roughness element. Further downstream, the traveling wave is a convective instability.

The influence of the initial transients on the traveling wave generation can be checked by the results plotted in figure 9. A Fourier transform in time (at the frequency $f = 3400\,\mathrm{Hz}$) and in z (at the spanwise wavenumber $2\beta_z$) has been performed on the DNS flow for each case. The amplitude of the corresponding chordwise velocity is plotted in figure 9 at a given chordwise location $s \approx 0.025\,\mathrm{m}$. The amplitude differs from one case to another, but it has been checked that the curves are proportional to each other. That means that in any studied case, the unsteady oscillation is a linear traveling crossflow wave $A\,q(n)\,\exp\left(2i\beta_z z + i\alpha s - 2i\pi f t\right)$, but with a different amplitude A. The value of this amplitude depends on the strength of the transient created by the initialization process, which especially decreases with the roughness height.

V. Conclusions

A Direct Numerical Simulation (DNS) of the flow around a roughness array placed on a swept cylinder has been carried out. A realistic configuration has been investigated: the roughness elements are not modelized but are meshed and no-slip conditions are directly imposed at their surface. Moreover, the DNS take into account the surface curvature. Four configurations with various roughness sizes have been studied. In any case, the height of the roughness elements is too small to directly trigger the turbulence, but high enough to induce non-linear receptivity phenomena. The computations show that both traveling and steady crossflow

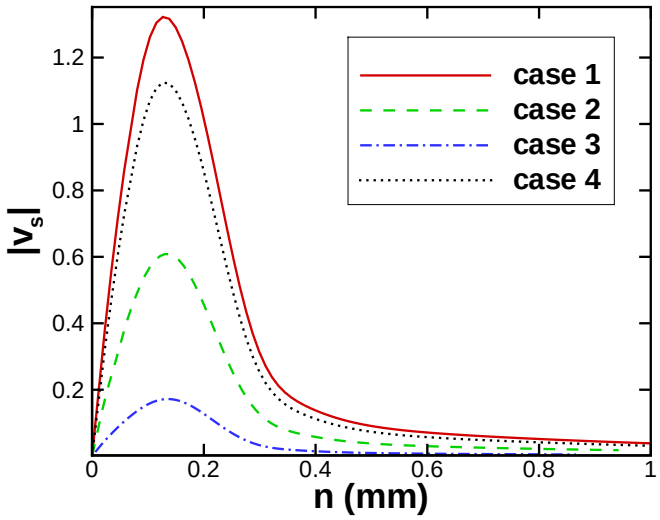

Figure 9. Amplitude functions for the chordwise velocity associated to the unsteady part of the perturbation, for each computation case (see Table 1). The chordwise location is $s/R_c \approx 14°$.

waves are generated downstream of the roughness array. The traveling waves seem to be excited by a pocket of absolute instability near the roughness location. Further downstream, this instability becomes convective, and the features of the traveling wave match perfectly those of the unsteady crossflow mode obtained by a linear stability analysis of the base flow. The amplitude of this traveling crossflow wave is fixed by transient effects during the initialization of the computation, which depend on the roughness dimensions. As this amplitude is high, the traveling wave non-linearly interacts with the stationary flow field. Therefore, the stationary wave generated downstream of the roughness elements differs from the steady crossflow mode that is predicted by the linear stability theory. It is thus difficult to quantify the receptivity of steady crossflow modes to large surface roughness.

VI. Acknowledgments

Part of the work described in the paper was carried out with the financial support of Airbus. The assistance of Marc Terracol in the use of the DNS code is gratefully acknowledged.

References

[1]Arnal, D., "Boundary layer transition: predictions based on linear theory," *AGARD FDP/VKI Special Course on 'Progress in Transition Modelling'*, AGARD R-793, VKI, Brussels, Belgium, 29 March - 1 April 1993, pp. 2.1–2.63.

[2]Saric, W.S. and Reed, H.L., "Crossflow instabilities - Theory & Technology," *AIAA-2003-771, 41st Aerospace Sciences Meeting & Exhibit*, Reno, NV, January 6-9 2003.

[3]Reibert, M.S. and Saric, W.S., "Review of swept-wing transition," *AIAA-97-1816, 28th Fluid Dynamics Conference*, Snowmass Village, CO, June 29-July 2 1997.

[4]Saric, W.S., Reed, H.L., and White, E.B., "Stability and transition of three-dimensional boundary layers," *Annu. Rev. Fluid Mech.*, Vol. 35, 2003, pp. 413–440.

[5]Bippes, H., "Basic experiments on transition in three-dimensional boundary layers dominated by crossflow instabilities," *Progress in Aerospace Sciences*, Vol. 35, 1999, pp. 363–412.

[6]Kachanov, Y.S., "Three-dimensional receptivity of boundary layers," *Eur. Jour. of Mech. B/Fluids*, Vol. 19, 2000, pp. 723–744.

[7]Choudhari, M. and Streett, C., "Boundary layer receptivity phenomena in three-dimensional and high-speed boundary

layers," *AIAA-90-5258, 2nd International Aerospace Planes Conference*, Orlando, FL, October 29-31 1990.

[8]Radeztsky, R.H., Reibert, M.S., and Saric, W.S., "Effect of isolated micron-sized roughness on transition in swept-wing flows," *AIAA Journal*, Vol. 37, No. 11, November 1999, pp. 1370–1377.

[9]Deyhle, H. and Bippes, H., "Disturbance growth in an unstable three-dimensional boundary layer and its dependence on environmental conditions," *J. Fluid Mech.*, Vol. 316, 1996, pp. 79–113.

[10]Crouch, J.D., "Receptivity of three-dimensional boundary layers," *AIAA-93-0074*, 1993.

[11]Choudhari, M., "Roughness-induced generation of crossflow vortices in three-dimensional boundary layers," *Theor. Comput. Fluid Dyn.*, Vol. 6, 1994, pp. 1–30.

[12]Ng, L.L. and Crouch, J.D., "Roughness-induced receptivity to crossflow vortices on a swept wing," *Phys. Fluids*, Vol. 11, No. 2, 1999, pp. 432–438.

[13]Bertolotti, F.P., "Receptivity of three-dimensional boundary-layers to localized wall roughness and suction," *Phys. Fluids*, Vol. 12, No. 7, 2000, pp. 1799–1809.

[14]Collis, S.S. and Lele, S.K., "Receptivity to surface roughness near a swept leading edge," *J. Fluid Mech.*, Vol. 380, 1999, pp. 141–168.

[15]Janke, E., "Receptivity and transition control of swept-wing boundary layers. Effects of surface curvature and nonlinearity," *AIAA-2001-2980, 31st AIAA Fluid Dynamics Conference & Exhibit*, Anaheim, CA, June 11-14 2001.

[16]Piot, E., Casalis, G., and Terracol, M., "Direct Numerical Simulation of the crossflow instabilities induced by a periodic roughness array on a swept cylinder : receptivity and stability investigations," *AIAA-2007-3976, 37th Fluid Dynamics Conference*, Miami, FL, June 25-28 2007.

[17]Tumin, A., "Multimode decomposition of spatially growing perturbations in a two-dimensional boundary layer," *Phys. Fluids*, Vol. 15, No. 9, 2003, pp. 2525–2540.

[18]Poll, D.I.A., "Some observations of the transition process on the windward face of a long yawed cylinder," *J. Fluid Mech.*, Vol. 150, 1985, pp. 329–356.

[19]Terracol, M., "Développement d'un solveur pour l'aéroacoustique numérique : sAbrinA," Tech. Rep. RT 5/07383 DSNA, Rapport technique ONERA, 2003.

[20]Terracol, M., Manoha, E., Herrero, C., Labourasse, E., Redonnet, S., and Sagaut, P., "Hybrid methods for airframe noise numerical prediction," *Theor. Comput. Fluid Dyn.*, Vol. 19, No. 3, 2005, pp. 197–227.

[21]Desquesnes, G., Terracol, M., Manoha, E., and Sagaut, P., "On the use of a high order overlapping grid method for coupling in CFD/CAA," *J. Comput. Phys.*, Vol. 220, No. 1, 2006, pp. 355–382.

[22]Saric, W.S., Hoos, J.A., and Radeztsky, R.H., "Boundary layer receptivity of sound with roughness," *First ASME JSME Fluids Engineering Conference*, Portland, Oregon, 1991.

[23]Casalis, G., Gouttenoire, C., and Troff, B., "Réceptivité localisée de la couche limite," C. R. Académie des Sciences, Paris, t. 325, Série IIb, 1997.